NJC

ROYAL SOCIETY OF CHEMISTRY

PAPER

View Article Online
View Journal | View Issue

Cite this: *New J. Chem.*, 2022, **46**, 20940

Photo-and thermoresponsive *N*-salicylideneaniline derivatives: solid-state studies and structural aspects†

Siya T. Hulushe, *[a] Frederick P. Malan, [b] Eric C. Hosten, [c] Kevin A. Lobb, [a] Setshaba D. Khanye [d] and Gareth M. Watkins[a]

N-Salicylideneaniline (SA) and its derivatives are known to possess chromism upon exposure to external stimuli. Herein, we present mechanochemical synthesis of a series of photo-and thermoresponsive SA-derivatives and report on solid-state stabilisation of their tautomeric forms either by change in temperature or by photoirradiation. The influence of UV light on proton transfer between the enol-imine (**EI**) and keto-amine (**KA**) forms was investigated at λ_1 = 254 and λ_2 = 365 nm. Differential scanning calorimetry (DSC) measurements provided extra information on the thermodynamic relationship between the prototropic tautomers, and their exposition to liquid nitrogen, combined with variable temperature single-crystal X-ray diffraction (VT-SCXRD) and spectroscopic data, ascertained structural reasons for the intrinsic thermo-optical properties of the compounds. A series of structural determinations between 150 and 300 K further shed light on the thermomechanical behaviour exhibited by the thermoresponsive compounds. By virtue of calorimetry we were able to demonstrate proton transfer *via* the intramolecular O···N hydrogen bond over the temperature range 193–453 K. This present work demonstrates the importance of applying complementary analytical techniques and appropriate approaches for understanding the switching behaviour between the **EI** and **KA** forms. Furthermore, the assertion that it is predominantly the planarity ($\varphi < 25^{\circ}$) that determines thermochromaticity is questioned.

Received 22nd June 2021,
Accepted 12th September 2022

DOI: 10.1039/d1nj03056f

rsc.li/njc

Introduction

Manipulating molecular switching properties of switchable species by external stimuli opens up ample opportunities in crystal engineering and materials sciences. With the increased interest in switching materials, in particular *N*-salicylideneanilines, it is not surprising that the experimental methods (*i.e.* the use of external stimuli) utilised to stabilise and isolate or separate these species have evolved. In principle, switching among tautomers induced by external stimuli can be exploited for biological or material applications, making the stabilisation and isolation of such materials in recent times a centre of attention.[1,2] These species have potential applications in optical storage, molecular switches, displays, signal, sensors, and optical data processing as well as numerous other photonic technologies.[3–6] Switching devices have been an important area of focus owing to their interesting performance in photochromism and thermochromism. Among switching devices, *N*-salicylideneaniline (SA) derivatives are well-known to possess excellent reversible photo- and thermochromism phenomena.[7–9] The mechanism of colour changes for SA-derivatives, to this point, has been carefully investigated and their generally recognised thermo- and photochromic processes are illustrated in Scheme 1.

When studying switching materials, the first two essential factors to look at are relative energies of their two (or more) forms as well as their structural differences. In the case of crystalline materials not only their respective molecular geometries (intramolecular interactions) but also the crystal packing, which characterise the spacing between the molecules and thus their intermolecular contacts, determine their switching properties.[10–14] The conventional mechanism for thermochromism is a temperature-dependent ground-state enol–keto

[a] *Department of Chemistry, Rhodes University, P. O. Box 94, Makhanda 6139, South Africa. E-mail: hulushesiya@gmail.com*
[b] *Department of Chemistry, University of Pretoria, 02 Lynwood Road, Hatfield, Pretoria 0002, South Africa*
[c] *Department of Chemistry, Nelson Mandela University, Summerstrand, P. O. Box 77000, Gqeberha 6031, South Africa*
[d] *Faculty of Pharmacy, Rhodes University, P. O. Box 94, Makhanda 6139, South Africa*

† Electronic supplementary information (ESI) available. CCDC 1899401, 1902658, 1966932, 1989369, 1989398, 1989403, 2014911, 2014914, 2019418, 2049690, 2049691, 2062423, 2157376, 2156456–2156467 and 2191107–2191119. For ESI and crystallographic data in CIF or other electronic format see DOI: **https://doi.org/10.1039/d1nj03056f**

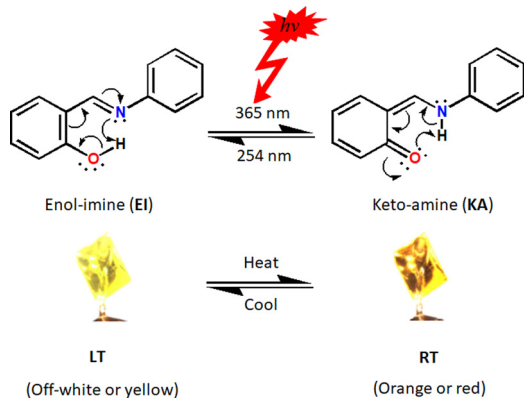

Scheme 1 Illustration of photochromism and thermochromism in a tautomeric *N*-salicylideneaniline.

tautomerisation *via* intramolecular proton transfer between the enol-imine (**EI**) and keto-amine (**KA**) forms.[15] Essentially, in solution, tautomers exist in rapid equilibrium with one another resulting in the formation of components that show similar physicochemical properties.[16] Additionally, tautomeric equilibria in solution are often manipulated by solvent polarity and proticity, pH and so forth.[17–20] Unlike in solution, in which different tautomeric forms coexist, usually only one tautomer emerges in solid-state. Few cases have been reported in which more than one tautomer appears in solid-state and these commonly include stoichiometric[21–23] or non-stoichiometric[24–27] mixtures displaying the same crystal. Even more scarce are examples in which both the enol–keto tautomeric forms are isolated in solid-state. However, the existence of a particular tautomer in the crystal depends, for the most part, on the parent molecule and the nature of the *N*-aryl substituent.[28] In addition, the electron-donor or acceptor ability of the *N*-aryl substituents, their size and position, as well as D–H···A (D = donor, A = acceptor) hydrogen bond characteristics, can facilitate stabilisation of one tautomer over the other.[29–32] Moreover, electron withdrawing substituents in the phenolic ring as well as an electron donating substituents in the aniline ring are known to stabilise the **KA** forms.[28] Generally, it has been suggested that thermochromic imines are planar (dihedral angle between aromatic subunits $\varphi < 25^\circ$) and photochromic ones are non-planar ($\varphi > 25^\circ$).[33–44] In this work, we have taken a step further by investigating this criterion in-depth.

Herein we wish to demonstrate that although containing $\varphi < 25^\circ$ for most of the compounds examined here, they are however non-thermochromic. In this work, we present the syntheses of a series of 5-nitrosalicylideneaniline derivatives, Fig. 1, with a few exhibiting reversible photochromic and/or thermochromic properties. The synthesised compounds were characterised by various analytical and spectroscopic techniques. Thermochromic properties of compounds **1–7** were elucidated by variable temperature single-crystal X-ray diffraction (VT-SCXRD). Enol–keto phase transitions were demonstrated by differential scanning calorimetry (DSC) experiments. The aim of the present work was to investigate the solid-state switching properties of the enol–keto tautomeric forms in

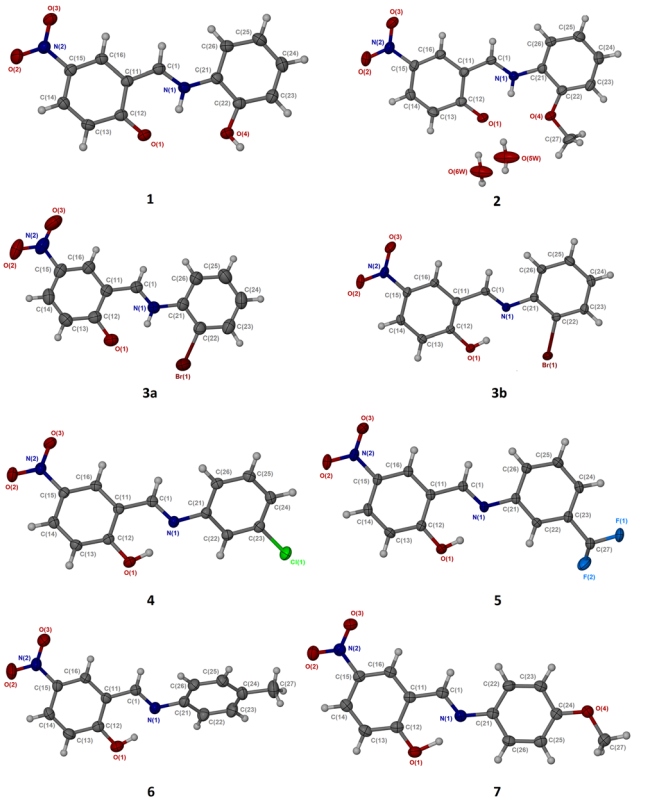

Fig. 1 ORTEP view and atom numbering scheme of compounds **1–7** with displacement ellipsoids drawn at 50% probability level. Hydrogen atoms are shown as off-white spheres with 0.2 Å radius.

response to external stimuli in the form of light and heat. In addition, a series of different electron-rich and electron-deficient aromatic substituents were selected to probe the role of the electron-acceptor strength on the physicochemical properties of prototropic tautomers – isomers that readily interconvert by the exchange of a proton preceded by the switch of a single and the conjugated double bond system.

Results and discussion

Synthesis and single-crystal X-ray diffraction

Mechanochemical syntheses of compounds **1–7** are discussed in the Experimental section (Fig. S1, ESI†). X-Ray crystallography analyses reveal that **1**, **4** and **7** crystallise in monoclinic $P2_1/n$ (No. 14) space group, while both **3** and **6** crystallise in space group $P2_1/c$ (No. 14); **2** and **5** crystallise in monoclinic systems with space groups $C2/c$ (No. 12) and $C2/m$ (No. 15), respectively. It is noteworthy to mention that the compounds are all non-centrosymmetric. Contrary to the rest of the structures, the keto-tautomeric form in **2** at 150 K (**2_LT**) and 298 K (**2_RT**) is stabilised by two water molecules as solvent of crystallisation. Compounds **1**, **2** and **3a** crystallise into the **KA** tautomeric forms and this is deduced from electron density mapping (Fig. S2, ESI†). For comparison, microscope images and superposition of similar compounds (employing the salicylaldimino moiety) are presented in Fig. 2 and 3. In contrast, **3b**, **4_LT**,

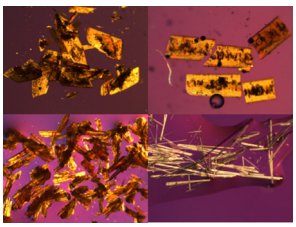

Fig. 2 Microscope image of single-crystals of compounds **1** (top left), **2** (top right), **3** (bottom left) and **4** (bottom right) obtained by recrystallisation from ethanol, water/methanol (0.5 : 0.5 v/v ratio) binary mixture, ethyl acetate/methanol (0.5 : 0.5 v/v ratio) and acetonitrile, respectively.

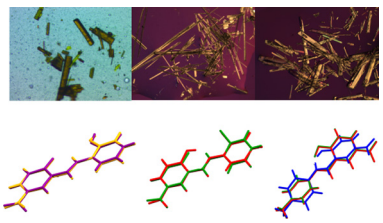

Fig. 3 Microscope images of compounds **5** (top left), **6** (top centre) and **7** (top right) obtained by recrystallisation from methanol, methanol/hexane mixture (0.5 : 0.5 v/v ratio) and chloroform, respectively, and the view of the molecular overlay of **1_LT** (purple) and **1_RT** (yellow) {bottom left}, **3a** (green) and **3b** (red) {bottom centre}, **6_LT** (red), **AYUGUX**[46] (blue) and **AYUGUX01**[47a] (green) {bottom right}.

4_RT, **5_LT** and **5_RT** are all enols, again deduced from electron density mapping (Fig. S2 and S3, ESI†) and their bond lengths (dO_{1-H1}) vary between 0.810(4) and 0.900(4) Å. Strong intramolecular hydrogen bonds are found between the N1 and O1 atoms with $d_{N1\cdots H1}$ bond lengths 1.830(2)–1.890(4) Å,[45] while the respective N···O distances are 2.582(8)–2.616(3) Å; the values for the ∠N1···H1–O1 angles are 146.50(4)° to 51.11(4)° (Table S1, ESI†). The bond lengths of the fragment N1═C1–C11═C12–O1 are indicative of electronic delocalisation (*i.e.* the C12–O1 bond lengths) with bond distances between 1.317(1) and 1.340(3) Å, and are also similar to the values observed for non-conjugated C–O bonds.[37]

The C1–C11 bond lengths are slightly shorter than the values observed for the corresponding bond in the **KA** tautomers, while the Csp^2–Csp^2 (C11–C12) bond length values are 1.269(1)–1.412(2) Å. Finally, C_{arom}–C═N–(C1═N1) bond lengths show values between 1.269(1) and 1.282(3) Å corresponding to C═N groups (1.301(11)) Å)[2]. Looking at the dihedral angles ($\varphi > 25°$) displayed by **4_LT**, **4_RT**, **6_LT** and **6_RT**, the compounds are anticipated to possess photochromic properties. This, however, shows that the so-called ''rule'': closed packing-only thermochromic is not obeyed. The first examples showing the ''rule'' breaking was exemplified in ref. 41–43.

Contrary to **AYUGUX**,[46] **AYUGUX01**[47a] and **MOSLUC**,[47b] crystallographic analysis indicates that the proton (H1 atom) attached to iminic N1 is disordered (by electron density mapping) with a small partial occupation factor of the second hydrogen bond position near the nitrogen atom in both **6** and **7**. Additionally, unlike **6_RT**, **7_LT** and **7_RT**, SCXRD data for **6_LT** show that the H1 seems to interact more with oxygen O1 atom rather than with the nitrogen N1 atom. In confirmation, and the O1–H1 or N1–H1 bond lengths are significantly shorter and longer with distances varying from 0.775(6) to 1.459(2) Å. Such intermediate values are consistent with average values between the corresponding bond lengths in **EI** and **KA** forms. Strong intramolecular hydrogen bonds between the N1 and O1 atoms with $d_{N1\cdots H1}$ bond lengths, the respective N···O distances and the values for the ∠N1···H1–O1 angles are similar to those described above.

The **Tα**, **Tβ** and torsion angles (Scheme S1, ESI†) for compounds **1–7** vary significantly while their packing indices are somewhat close. Packing index could not be determined for compound **5_RT** which exhibits a typical disorder in the F1, F2 and F3 atoms of the trifluoromethyl group. However, compounds **3a** and **3b** showed significantly different packing indices confirming the existence of these two tautomeric forms. Although compounds **1–4**, **6** and **7** display strong intramolecular hydrogen bonds that ''fix'' planarity in their corresponding salicylaldimino moieties, owing to the non-aromatic nature of the substituent at the imino nitrogen, the compounds are non-planar and of course compound **5** (completely planar) is an exception (see dihedral angles in Table S2, ESI†). The crystal packing in **1–7**, Fig. S4, ESI,† is locked by various strong intermolecular hydrogen bonds between adjacent molecules generating different supramolecular synthons.

Solid-state studies

The infrared (IR) spectra of compounds **3b**, **4**, and **5** displayed typical O–H, C═N, and C–O stretching vibrations for enol-imines.[48–52] In contrast to the above assignment, the medium-strong bands in the lower wavelength range 3300–2500 cm^{-1} correspond to N–H stretching frequencies for compounds **1**, **2** and **3a**. Nonetheless, there was not enough evidence that could be deduced from the IR spectra substantiating that compounds **6** and **7** exist as either a **KA** or **EI**. Among the chemical signals which aided us in distinguishing the tautomeric forms, the most sensitive in solid-state (SS) ^{13}C NMR spectra is the shift related to the carbon atom (here tagged C12) bearing the keto or enol functionality.

Ideally, for the **KA** form this signal appears at *ca* 180 ppm, whereas for the **EI** form it is expected to shift to *ca* 160 ppm.[53,54] Solid-state ^{13}C cross-polarisation/magnetic angle spinning (CP/MAS) NMR experiments (Fig. 4) showed a significantly different set of signals especially for C1 and C12 (included in the intramolecular OH···N/NH···O hydrogen bond). The chemical signals were assigned by means of cross-polarisation from ^{1}H to ^{13}C (hC.CP) SS NMR method. As with previous research groups,[53,54] the ^{13}C (CP/MAS) NMR signals belonging to C1 (imine carbon) and C12 carbon atoms appear at 167.5 and 178.5 ppm in **3b** while the signals in **3a** are observed at 173.5 and 216.4 ppm, respectively. These outcomes, together with the SCXRD studies, clearly demonstrated that compound **3b** exists as an **EI** while **3a** is its **KA** tautomer.

Fig. 5 depicts differential scanning calorimetry (DSC) measurements for **3b**, **4** and **5** at the temperature ranging from

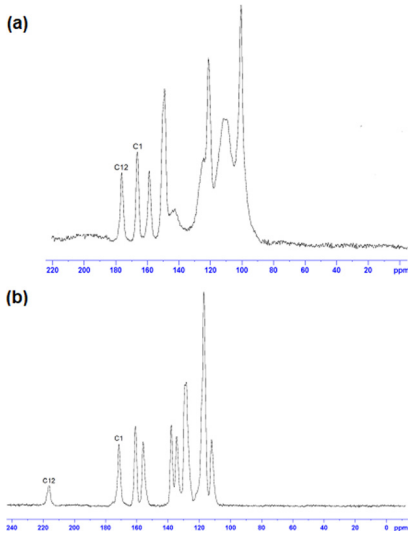

Fig. 4 Solid-state ^{13}C (CP/MAS) NMR spectra of (a) compound **3a** and (b) compound **3b**.

193 K to 453 K. Enol–keto (**3b** → **3a**) and keto–enol (**3a** → **3b**) were observed by a small endotherm at 374 K (single-step phase transition) and, exotherms at 354 K and 375 K (two-step phase transformation; highlighted pink in Fig. 5a), respectively, under heat-cool conditions. The melting curve for **3b** show a temperature arrest at 415 K (region highlighted orange) and there exist a slow solidification process in the DSC cooling trace at 396 K (highlighted light-blue).

Compound **4** and **5** exhibited similar enol → keto → enol phase transformations, slow solidification and 'melts' certainly with different thermal events. On heating, **4** and **5** demonstrated exothermic peaks at 420 K and 376 K, respectively, with corresponding endotherms at 306 K and 270 K on subsequent cooling.

All the above experiments were performed multiple times with identical results (reversible conversions were observed infinite times through consecutive heating and cooling cycles using closed aluminium caps).

Furthermore, DSC profiles using open caps (ESI†) revealed shallow exotherms in the range 441–573 K which were assigned to melting points of the compounds. Among the samples, **1** showed the highest melting point (onset: 573 K), with **3b** and **7** displaying almost identical 'melts' (onset: 471 K), whilst the melting points of the other samples indicated stronger/weaker intermolecular interactions stabilising their crystal structures (onsets: **2** 490 K; **4** 503 K; **5** 441 K; **6** 461 K).

Photoirradiation

Upon single-crystal-to-single-crystal (SCSC) ultraviolet (UV) light irradiation (at 365 nm for 48 hours), significant dissimilarities were observed in the solid-state UV-visible absorption

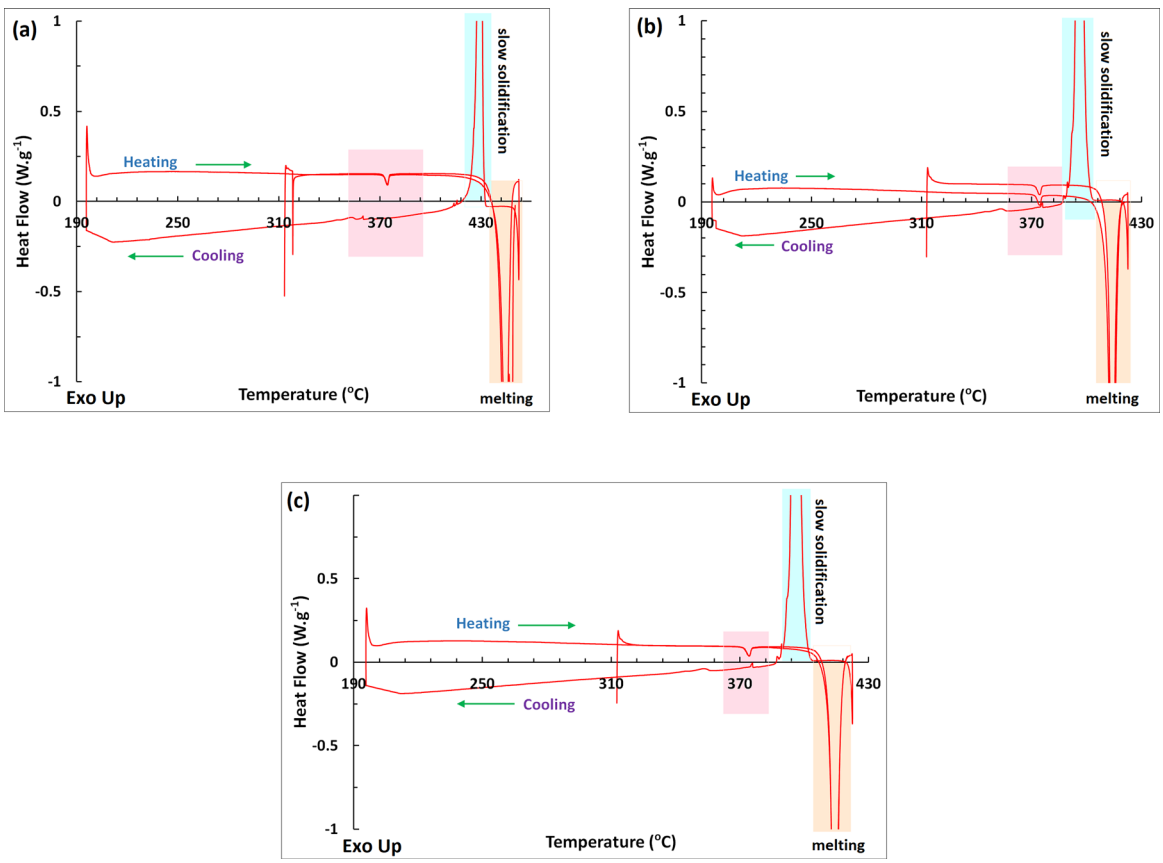

Fig. 5 Heating-cooling truncated DSC curves (Exotherm Up) for compounds (a) **3b**, (b) **4** and (c) **5**.

Table 1 Stimuli stabilising the investigated compounds

	Stimuli			
	Temperature		Heat/light	
Compound	LT (K)	RT (K)	Chromism	
1	150	298	—	—
2	150	298	—	—
3	150	298	Photo[a]	Thermo
4	150	298	—	Thermo
5	150	298	—	Thermo
6	150	298	—	—
7	150	298	—	—

[a] SCSC photoirradiation at 365 nm.

spectra, in particular for **3a** and **3b**. Before UV light irradiation, the spectrum of **3b** showed a small peak at 480 nm, and no profound absorption at *ca.* 500 nm. Essentially, a new peak (accompanied by colour change from orange to light yellow) emerged at about 500 nm for the photoinduced crystals of **3b** suggesting enol → keto structural transformation to form **3a**. However, UV-visible spectra did not display significant changes in the absorption bands for the other imines. This implies that compound **3** is photochromic while the rest are non-photochromic (Table 1).

Thermochromism

The thermochromic properties of the compounds were investigated by repeated exposure to a temperature change from room to liquid-nitrogen temperature. The powdered forms of the imines were placed in test tubes and submerged into liquid nitrogen (at 77 K), while the thermal responsive single-crystals of compounds **3b**, **4** and **5** were studied at 150, 180, 210, 240, 270 and 300 K. The results for crystalline and powdered forms (Fig. S5, ESI†) show that these compounds are reversibly thermochromic. The crystal colours of **3b** and **5** both changed from orange to pale orange upon heating from 150 to 300 K (Fig. 6), while their powdered forms became pale yellow and yellow at 77 K, respectively. On heating from 150 up to 300 K, the colour of the crystal of **4** changed from brown to yellow-brown, while the colour of its powder was brown-green at **RT** and became paler upon cooling to 77 K.

Crystallographic details of compounds **3b**, **4** and **5** from 100 K, 140 K, 150–300 K are presented in Tables S3–S7 (ESI†). Analysis of the diffraction patterns showed that the lengths of *a*-, *b*- and *c*-axes along with the β angle increase with temperature in the case of **3b**. For **4**, β angle contraction is accompanied by volume expansion upon heating while the unit cell edges experience linear positive thermal expansion (PTE). In compound **5**, large PTE along *c*- and *b*-axes occurs with increasing temperature, whereas *a*- shows an uncommon behaviour of contracting (uniaxial negative thermal expansion; NTE). The thermal expansion along the *a*-axis is negative, but small in comparison to the expansion along *b*- and *c*-, therefore globally the volume increases with temperature. We established that these changes are only reversible in the range 150–240 K for **3b**, as confirmed by unit cell determinations at this temperature range. The trend of unit cell parameter changes from 150 to 300 K is plotted in Fig. 7 for compounds **3b**, **4** and **5**. For **3b**, **4** and **5** in the 150–300 K range, principal axes and linear expansion coefficient were calculated utilising the programme *PASCal*.[55] Thermal expansion coefficients of compounds **3b**, **4** and **5** within the temperature range 150–300 K are summarised in Table S8 (ESI†). Fig. 8 illustrates how the principal axes lengths change with increasing temperature for **3b**, **4** and **5** along with the expansivity/compressibility plots for the principal axes *X*1, *X*2 and *X*3. The PTE of the *a*-, *b*- and *c*-axes in **3b** are relatively small—the coefficients of linear thermal expansion (in MK^{-1}) over the temperature range 150–300 K are 13.0; 35.0 and 149 for *X*1, *X*2 and *X*3, respectively. The volume-thermal-expansion coefficient α_v (102.7 MK^{-1} on average) for **3b** is about $1\frac{1}{4}$ times larger than for ice, but almost 5 times smaller than for methanol monohydrate.[56] The major part of the expansion in **4** is along the *c*-axis with thermal expansion coefficients α_a = 21.8;

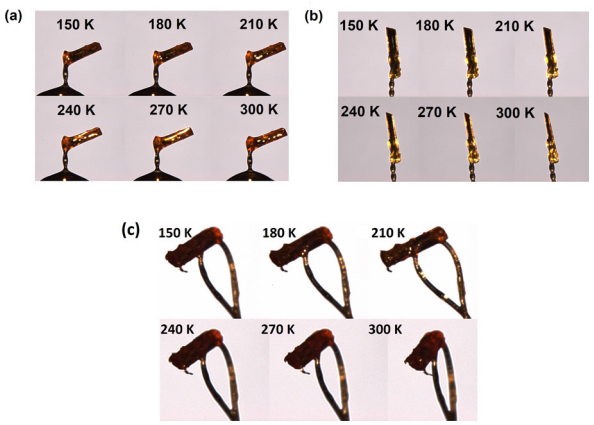

Fig. 6 Photograph images of thermochromic crystals of (a) **3b**, (b) **4** and (c) **5** at 150–300 K.

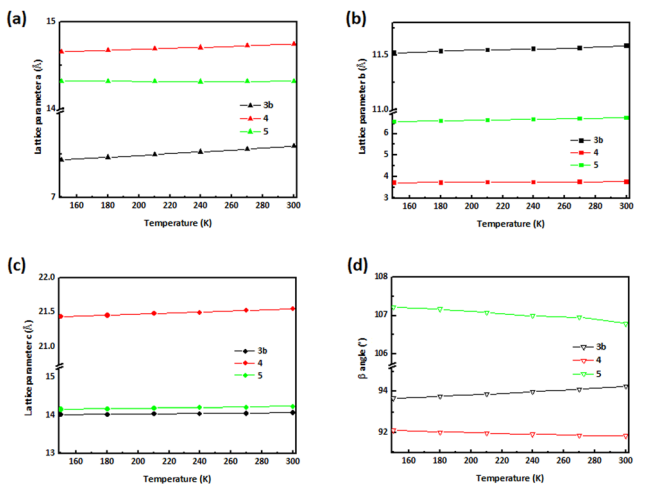

Fig. 7 The effect of temperature on structural parameters. Structural determinations were repeatedly collected for the same crystal, starting at 150–300 K, heating the crystal by 30 K between successive data sets. Temperature dependences of (a) *a*-, (b) *b*-, (c) *c*-axes and (d) β angles of **3b**, **4** and **5**.

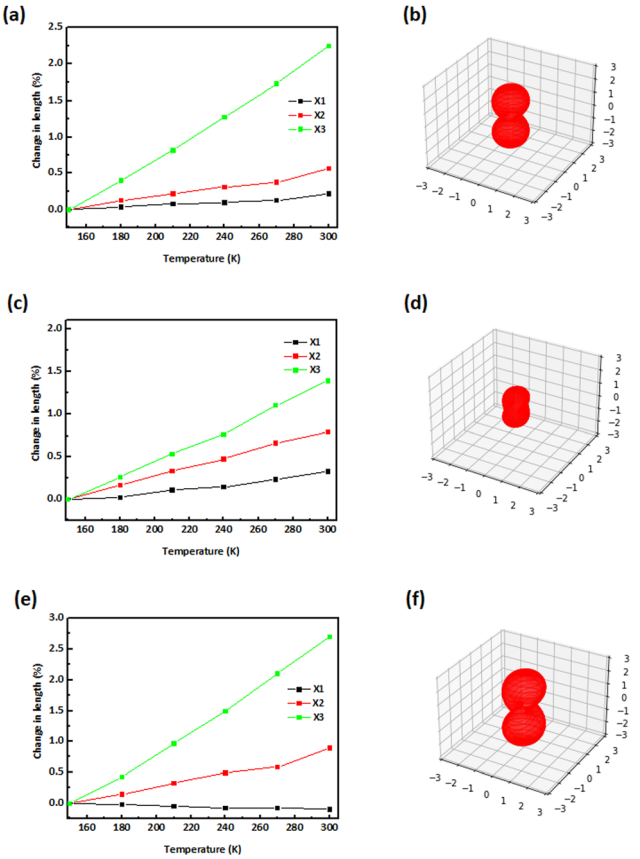

Fig. 8 Percentage changes in principal axis lengths as a function of temperature along with the expansivity/compressibility plots for the principal axes *X*1, *X*2 and *X*3 for (a and b) **3b**, (c and d) **4** and (e and f) **5**.

α_b = 53.2 and α_a = 92.7 MK^{-1} along the *X*1, *X*2 and *X*3, respectively. The coefficient of volumetric thermal expansion is 169.4 MK^{-1}. A thermal expansion study of **5**, aimed at characterising its mechanical anisotropy, revealed a large difference in the lattice coefficients of thermal expansion: −6.4, 56.5 and 181.4 MK^{-1} for *X*1, *X*2 and *X*3, respectively, while the coefficient of volumetric thermal expansion is 233.9 MK^{-1}. The low value along the *a*-axis indicates the "*hard*" direction of the crystal, along which the intermolecular interactions are strongest, highlighting the presence of hydrogen bonds along a; thus, in this direction, molecules experience strong van der Waals forces. The hydrogen-bond structure in **3b**, **4** and **5** is preserved, because no phase change has been observed over the range 150–300 K; essentially, it is presumed that there exist a concerted movement of molecules to optimise the van der Waals forces along the crystallographic *a*-axis.

Conclusions

Herein we present solid-state insights into photo-and thermochromism in a series of selected *N*-salicylideneaniline derivatives. This work focused on an in-depth structural characterisation, combining differential scanning calorimetry (DSC), variable temperature single-crystal X-ray diffraction (VT-SCXRD) and spectroscopic data. The molecules studied here are almost planar (0 < dihedral angle (φ) < 8.31(9)°), of course compounds **4** and **6** are exceptions, and are presented as either enol-imines or keto-amines.

In addition, the electron withdrawing character of the *N*-aryl substituents at 2-position facilitated stabilisation of keto-imines.

Formation of intermolecular hydrogen bonding and further aggregation of the hydrogen-bonded clusters participated as a stimulant for the temperature-induced shift to the tautomer that is less stable. A detailed structural study of the compounds has led us to the opinion that the thermochromic properties and enol–keto tautomerism are governed by supramolecular influences. Furthermore, ultraviolet-induced single-crystal-to-single-crystal (SCSC) transformation assisted enol-to-keto tautomerism in **3**. In this regard, compound **5** exhibited partial negative thermal expansion (NTE) while both **3** and **4** demonstrated positive thermal expansion (PTE) together with thermochromism and, photochromism in the case of **3**. However, there exist some examples where the so-called "rule": closed packing-only thermochromic behaviour was not obeyed in the present account. It has been shown here that, with proper control, multiple responsive switching materials can be achieved. Essentially, SA-derivatives of this nature can be exploited as ultraviolet strength sensors for naked eye detection of UV radiation pollution. In addition, tuning of thermoresponsive materials holds promise in further applications such as non-expansive electronics and thermomechanical devices.

Experimental section

General

Materials; 5-nitrosalicylaldehyde, *o*-aminophenol, *o*-anisidine, *o*-bromoaniline and *m*-chloroaniline, *m*-(trifluoromethyl)-aniline, *p*-toluidine and *p*-anisidine were sourced from Sigma-Aldrich (Pty) Ltd and Merck (Pty) Ltd with >99% chemical purity. NMR solvents (acetone-d_6, $CDCl_3$ and DMSO-d_6) were sourced from Sigma-Aldrich (Germany) with >98% chemical purity. Other solvents utilised; DMSO, ethanol, ethyl acetate and hexane were from Protea Chemicals (South Africa) while chloroform was obtained from BM Scientific/Parow Industria (South Africa). Methanol from Merck (Germany) and acetonitrile from Ranbaxy Fine Chemicals Ltd (India) of high-performance liquid chromatography (HPLC) grade. All these chemicals were commercially available and used without further purification.

Synthesis of the compounds

Mechanochemical syntheses were performed at room temperature (**RT**; 298 K) and at 40–50% relative humidity. In all cases, equimolar amounts of 5-nitrosalicylaldehyde (1.0 mmol) and the respective anilines (1.0 mmol) were used in order to obtain the SA-derivatives. Neat grinding (NG) of **1**–**7** in an agate mortar led, in most cases, first to yellow/orange moist paste-like

reaction mixtures, which started to solidify after 0–25 min and the crystalline solids were obtained in 57–70% yields. For each of the compounds, the simulated SCXRD patterns corresponded with that of PXRD which indicated that the Schiff bases were obtained as pure crystalline phases.

Photoirradiation

The single-crystal samples were irradiated for 24 hours (UV lamp, long wavelength at λ_1 = 365 nm and short wavelength at λ_2 = 254 nm, 6.0 watt of full intensity).

Synthesis of 1. 2-((*E*)-(2-hydroxyphenyliminio)methyl)-4-nitro-phenolate was synthesised by neat grinding (NG) of equimolar amounts of *o*-aminophenol and 5-nitrosalicylaldehyde. Orange platelets of **1**, suitable for SCXRD analysis, were obtained by slow evaporation from a saturated solution of ethanol after 5 days. Yield 70%; M.P: (onset temperature observed by DSC and confirmed using a Reichert Hot-Stage melting point apparatus) 573 K, MW: 258.24 g mol^{-1}. IR: ν_{max} (ATR, cm^{-1}): 3495–3283 (br, O–H), 3449 (m, N–H), 3061 (s, C–H), 1616 (s, C═N), 1582, 1469 (s, C═C$_{arom}$), 1307 (s, N–O$_2$), 1176 (s, C–O). UV-visible: λ_{max} (nm) (ε, M^{-1} cm^{-1}) (band assign.) ($CHCl_3$): 446 (628) (n–π*), 366 (1234) (n–π*), 279 (6336) (π–π*), 241 (7710) (CT). ^{1}H NMR (DMSO-d$_6$, 400 MHz) δ (ppm): exp. 6.94–6.98 (4H, m, ArH), 7.23 (1H, m, ArH), 7.58–7.62 (1H, m, ArH), 8.17 (1H, dd, J = 9.4 Hz and J = 2.9 Hz, ArH), 8.61 (1H, d, J = 2.9 Hz, CH═N), 9.30 (1H, s, O–H), 10.39 (1H, s, N–H); 15.72 (1H, s, O–H); 13C (DMSO-d$_6$, 400 MHz) (δ ppm): 116.9, 117.06, 119.2, 120.3, 121.0, 129.2, 129.8, 130.2, 130.9, 137.2, 150.9 (ArC), 159.7 (PhCH═N), 173.0 (ArC). HRMS (ESI) m/z calculated for $C_{13}H_{11}N_2O_4$ 259.0719, found 259.0711 [M + H$^+$]. Anal. calcd C, 60.47; H, 3.90; N, 10.9%. Found. C, 60.52; H, 3.88; N, 10.9%.

Synthesis of 2. 2-((*E*)-(2-Methoxyphenyliminio)methyl)-4-nitro-phenolate was synthesised by NG of equimolar amounts of *o*-anisidine and 5-nitrosalicylaldehyde. Red-orange prisms of the dihydrated form of compound **2**, suitable for SCXRD analysis, were obtained by slow evaporation from a saturated water/methanol (0.5 : 0.5 v/v ratio) mixture after 2 weeks. Yield 68%; M.P: 490 K, MW: 272.27 g mol^{-1}. IR ν_{max} (ATR, cm^{-1}): 3500–3185 (br, O–H), 3445 (s, N–H), 3056 (s, C–H), 1617 (s, C═N), 1554, 1463 (s, C═C$_{arom}$), 1312 (s, N–O$_2$), 1178 (s, C–O). UV-visible: λ_{max} (nm) (ε, M^{-1} cm^{-1}) (band assign.) ($CHCl_3$): 449 (1168) (n–π*), 350 (4366) (n–π*), 295 (15 280) (π–π*), 238 (16 314) (CT). ^{1}H NMR ($CDCl_3$, 400 MHz) δ (ppm): 3.88 (3H, s, OCH_3), 6.95–7.00 (3H, m, ArH), 7.24–7.28 (2H, t, J = 8.2 Hz, ArH), 8.15–8.18 (1H, d, J = 12.0 Hz, ArH), 8.30–8.31 (1H, d, J = 2.8 Hz, CH═N), 8.74 (1H, s, ArH), 15.31 (1H, s, O–H); ^{13}C ($CDCl_3$, 400 MHz) (δ ppm): 57.1 ($PhOCH_3$), 112.3, 117.5, 118.8, 120.0, 122.1, 128.9, 129.7, 134.9, 139.9, 153.5, 160.1 (PhCH═N), 169.7 (ArC). HRMS (ESI) m/z calculated for $C_{14}H_{13}N_2O_4$ 273.0875, found 273.0873 [M + H$^+$]. Anal. calcd C, 61.76; H, 4.44; N, 10.3%. Found. C, 61.66; H, 4.42; N, 10.4%.

Synthesis of 3a. 2-((*E*)-(2-Bromophenyliminio)methyl)-4-nitro-phenolate was prepared by single-crystal-to-single-crystal (SCSC) UV light irradiation (365 nm, 5 mW cm^{-2}) of compound **3b**. Yield 100%; M.P: 471 K, MW: 321.13 g mol^{-1}. IR ν_{max} (ATR, cm^{-1}): 3467 (s, N–H), 3078 (m, C–H), 1605 (s, C═N), 1561, 1472 (s, C═C$_{arom}$), 1378 (s, N–O$_2$), 1738, 1173 (s, C–O). UV-visible: λ_{max} (nm) (ε, M^{-1} cm^{-1}) (band assign.) (MeOH): 361 (1871) (n–π*), 247 (2043) (n–π*), 207 (2248) (CT). ^{1}H NMR ($CDCl_3$, 400 MHz) δ (ppm): 7.21–7.25 (3H, m, ArH), 7.34–7.38 (4H, m, ArH), 10.3 (1H, s, CH═N), 11.6 (1H, s, N–H); ^{13}C (DMSO-d$_6$, 400 MHz) (δ ppm): 107.9, 115.9, 117.8, 118.9, 122.6, 124.8, 128.7, 131.1, 132.5, 140.2, 146.2, 166.2 (PhCH═N), 189.5 (ArC═O). HRMS (ESI) m/z calculated for $C_{13}H_{10}N_2O_3Br$ 320.9875, found 320.9872 [M + H$^+$]. Anal. calcd C, 48.62; H, 2.83; N, 8.73%. Found. C, 48.65; H, 2.78; N, 8.76%.

Synthesis of 3b. 2-((*E*)-(2-bromophenylimino)methyl)-4-nitro-phenol was synthesised by NG of equimolar amounts of *o*-bromoaniline and 5-nitrosalicylaldehyde. Orange block-shaped crystals of **3b**, suitable for SCXRD analysis, were obtained by slow evaporation from a saturated solution of ethyl acetate/methanol mixture after 3 days. Yield 67%; M.P: 471 K, MW: 321.13 g mol^{-1}. IR ν_{max} (ATR, cm^{-1}): 3483–3259 (br, O–H), 3058 (m, C–H), 1609 (s, C═N), 1550, 1470 (s, C═C$_{arom}$), 1354 (s, N–O$_2$), 1176 (sh, C–O). UV-visible: λ_{max} (nm) (ε, M^{-1} cm^{-1}) (band assign.) ($CHCl_3$): 448 (1242) (n–π*), 344 (9693) (n–π*), 271 (11 334) (π–π*), 239 (16 143) (CT). ^{1}H NMR ($CDCl_3$, 400 MHz) δ (ppm): 7.57 (1H, t, J = 7.7 Hz, ArH), 7.70 (1H, ddd, J = 7.8 Hz, J = 4.8 Hz and J = 1.4 Hz, ArH), 7.81 (1H, d, J = 8.0 Hz, ArH), 8.35–8.37 (2H, ddd, J = 9.2 Hz, J = 2.7 Hz and J = 0.8 Hz, ArH), 8.45–8.47 (1H, dd, J = 9.2 Hz and J = 2.8 Hz, ArH), 8.67 (1H, d, J = 2.7 Hz, CH═N), 9.22 (1H, d, J = 8.5 Hz, ArH), 14.27 (1H, s, O–H). ^{1}H NMR (acetone-d$_6$, 400 MHz) δ (ppm): 7.06 (1H, d, J = 9.2 Hz, ArH), 7.13–7.25 (2H, m, ArH), 7.34–7.38 (1H, td, J = 7.9 Hz and J = 1.1 Hz, ArH), 7.63–7.65 (1H, dd, J = 7.9 Hz and J = 1.02 Hz, ArH), 8.20–8.23 (1H, dd, J = 9.2 Hz and J = 2.7 Hz, ArH), 8.35 (1H, d, J = 2.7 Hz, CH═N), 8.64 (1H, s, ArH), 14.06 (1H, s, O–H); ^{13}C (DMSO-d$_6$, 400 MHz) (δ ppm): 118.5, 119.1, 119.9, 120.5, 129.0, 129.2, 129.6, 129.7, 133.5, 140.0, 145.5, 163.3 (PhCHN), 166.3 (ArC). HRMS (ESI) m/z calculated for $C_{13}H_{10}N_2O_3Br$ 320.9875, found 320.9867 [M + H$^+$]. Anal. calcd C, 48.62; H, 2.83; N, 8.73%. Found. C, 48.59; H, 2.78; N, 8.80%.

Synthesis of 4. 2-((*E*)-(3-chlorophenylimino)methyl)-4-nitro-phenol was synthesised by NG of equimolar amounts of *m*-chloroaniline and 5-nitrosalicylaldehyde. Yellow needles of **4**, suitable for SCXRD analysis, were obtained by slow evaporation from a saturated solution of acetonitrile after one week. Yield 61%; M.P: 503 K, MW: 276.68 g mol^{-1}. IR ν_{max} (ATR, cm^{-1}): 3074 (s, C–H), 1617 (s, C═N), 1568, 1473 (s, C═C$_{arom}$), 1389 (s, N–O$_2$), 1183 (s, C–O). UV-visible: λ_{max} (nm) (ε, M^{-1} cm^{-1}) (band assign.) ($CHCl_3$): 453 (891) (n–π*), 354 (14 758) (n–π*), 240 (16 283) (CT). ^{1}H NMR ($CDCl_3$, 400 MHz) δ (ppm): 7.04–7.15 (2H, m, ArH), 7.26–7.32 (3H, m, ArH), 8.21–8.23 (1H, dd, J = 9.1 Hz and J = 2.4 Hz, ArH), 8.34–8.35 (1H, d, J = 2.5 Hz, CH═N), 8.64 (1H, s, ArH), 13.9 (1H, s, O–H); ^{13}C ($CDCl_3$, 400 MHz) (δ ppm): 118.0, 118.4, 119.6, 121.5, 127.9, 128.6, 128.7, 130.7, 135.4, 148.3, 161.9 (ArC), 166.5 (PhCH═N), 207.0 (ArC═O). HRMS (ESI) m/z calculated for $C_{13}H_{10}N_2O_3Cl$ 277.0379, found 277.0374 [M + H$^+$]. Anal. calcd C, 56.43; H, 3.28; N, 10.1%. Found. C, 56.47; H, 3.21; N, 10.4%.

Synthesis of 5. 2-((*E*)-(3-(Trifluoromethyl)phenylimino)-methyl)-4-nitrophenol was synthesised by NG of equimolar amounts of *m*-(trifluoromethyl)aniline and 5-nitrosalicyl-aldehyde. Orange rod-like crystals of **5**, suitable for SCXRD analysis, were obtained by slow evaporation from a saturated solution of methanol after 8 days. Yield 59%; M.P: 441 K, MW: 310.23 g mol^{-1}. IR ν_{max} (ATR, cm^{-1}): 3068 (m, C–H), 1622 (sh, C═N), 1568, 1471 (s, C═C_{arom}), 1384 (s, N–O_2), 1729, 1187 (s, C–O). UV-visible: λ_{max} (nm) (ε, M^{-1} cm^{-1}) (band assign.) ($CHCl_3$): 448 (973) (n–π*), 361 (14 950) (n–π*), 242 (16 269) (CT). ^{1}H NMR (DMSO-d_6, 400 MHz) δ (ppm): 7.15–7.23 (1H, t, J = 9.9 Hz, ArH), 7.69–7.76 (3H, m, ArH), 7.83 (1H, s, ArH), 8.67–8.66 (1H, dd, J = 9.2 Hz and J = 2.9 Hz, CH═N), 8.69 (1H, d, J = 2.9 Hz, ArH), 9.18 (1H, s, ArH), 13.6 (1H, s, N–H); ^{13}C (DMSO-d_6, 400 MHz) (δ ppm): 118.5, 119.5, 124.2, 128.4, 129.1, 130.6, 130.9, 131.1, 140.0, 148.8, 163.3 (ArC), 166.2 (PhCH═N), 189.5 (ArC═O). HRMS (ESI) m/z calculated for $C_{14}H_{10}N_2O_3F_3$ 311.0643, found 311.0641 [M + H^+]. Anal. calcd C, 54.20; H, 2.92; N, 9.03%. Found. C, 54.22; H, 2.89; N, 9.01%.

Synthesis of 6. 2-((*E*)-(*p*-Tolylimino)methyl)-4-nitrophenol was synthesised by NG of equimolar amounts of *p*-toluidine and 5-nitrosalicylaldehyde. Orange needles of **6**, suitable for SCXRD analysis, were obtained by slow evaporation from a saturated solution of methanol/hexane mixture (0.5 : 0.5 v/v ratio) after 2 days. Yield 63%; M.P: 461 K, MW: 256.26 g mol^{-1}. IR ν_{max} (ATR, cm^{-1}): 3500–3245 (m, O–H), 3455 (s, N–H), 3075 (sh, C–H), 1603 (s, C═N), 1555, 1470 (s, C═C_{arom}), 1377 (s, N–O_2), 1737, 1174 (s, C–O). UV-visible: λ_{max} (nm) (ε, M^{-1} cm^{-1}) (band assign.) ($CHCl_3$): 445 (1087) (n–π*), 341 (13 205) (n–π*), 309 (14 248) (n–π*), 267 (13 366) (π–π*), 240 (16 250) (CT). ^{1}H NMR ($CDCl_3$, 400 MHz) δ (ppm): 2.33 (3H, s, CH_3), 6.99–7.01 (1H, d, J = 9.5 Hz, ArH), 7.25–7.28 (2H, m, ArH), 8.16–8.19 (1H, dd, J = 9.2 Hz and J = 2.7 Hz, ArH), 8.30 (1H, d, J = 2.7 Hz, CH═N), 8.63 (1H, s, ArH), 14.55 (1H, s, O–H); ^{13}C (DMSO-d_6, 400 MHz) (δ ppm): 21.1 ($PhCH_3$), 118.8, 118.9, 121.7, 128.7, 129.1, 130.5, 138.0, 139.3, 143.8 (ArC), 161.2 (PhCH═N), 167.9 (ArC). HRMS (ESI) m/z calculated for $C_{14}H1_3N_2O_3$ 257.0926, found 257.0924 [M + H^+]. Anal. calcd C, 65.62; H, 4.72; N, 10.9%. Found. C, 65.63; H, 4.69; N, 11.2%.

Synthesis of 7. 2-((*E*)-(4-Methoxyphenylimino)methyl)-4-nitro-phenol was synthesised by NG of equimolar amounts of *p*-anisidine and 5-nitrosalicylaldehyde. Yellow needles of **7**, suitable for SCXRD analysis, were obtained by slow evaporation from a saturated solution of chloroform after 3 days. Yield 57%; M.P: 471 K, MW: 272.27 g mol^{-1}. IR ν_{max} (ATR, cm^{-1}): 3500–3335 (s, O–H), 3443 (m, N–H), 305 (s, C–H), 1611 (s, C═N), 1555, 1472 (s, C═C_{arom}), 1365 (s, N–O_2), 1733, 1179 (s, C–O). UV-visible: λ_{max} (nm) (ε, M^{-1} cm^{-1}) (band assign.) ($CHCl_3$): 439 (916) (n–π*), 355 (11 090) (n–π*), 274 (14 507) (π–π*), 239 (16 257) (CT). ^{1}H NMR (DMSO-d_6, 400 MHz) δ (ppm): 3.81 (3H, s, CH_3), 7.04–7.09 (3H, t, J = 8.6 Hz, ArH), 7.48–7.51 (2H, d, J = 8.8 Hz, ArH), 8.20–8.24 (1H, d, J = 12.04 Hz, ArH), 8.61 (1H, s, CH═N), 9.15 (1H, s, ArH), 14.7 (1H, s, O–H); ^{13}C (DMSO-d_6, 400 MHz) (δ ppm): 55.9 ($PhOCH_3$), 115.3, 118.79, 118.9, 123.3, 128.5, 128.9, 139.1, 139.3 (ArC), 159.6 (PhCH═N), 159.8 (ArC), 167.7 (ArC). HRMS (ESI) m/z calculated for $C_{14}H_{13}N_2O_4$ 273.0875, found 273.0873 [M + H^+]. Anal. calcd C, 61.76; H, 4.43; N, 10.3%. Found. C, 61.79; H, 4.39; N, 10.3%.

Characterisation

IR spectroscopy. All infrared (IR) spectra (Fig. S6, ESI†) were collected on a PerkinElmer Spectrum 100 Fourier-transform IR spectrometer with a KBr beam splitter and fitted with an attenuated total reflection (ATR) attachment. Mid-infrared spectra with frequency of 4000–650 cm^{-1} were obtained by placing samples on a diamond/ZnSe crystal plate and using the force gauge between 100 and 149. The instrument runs an average of four scans with 4 cm^{-1} resolution and 128 cycles for both background and measurements. Samples were baseline corrected and smoothed using Spectrum *version* 6.3.5 software.

NMR spectroscopy. ^{1}H and ^{13}C NMR spectral data were collected using a Bruker Avance III HD 400 MHz NMR with liquid probe and 600 MHz NMR (with a cryoprobe for variable-temperature measurements) spectrometers with tetramethylsilane (TMS) as an internal reference. Spectra were recorded in deuterated solvents: acetone-d_6, $CDCl_3$ and DMSO-d_6. All chemical shift values are reported in parts per million (ppm) referenced to residual solvent resonances (acetone δ_H 2.09, δ_C 205.87; $CDCl_3$ δ_H 7.26, δ_C 77.36; DMSO δ_H 2.50, δ_C 39.5). The coupling constants are given in Hertz. Signal multiplicity patterns are abbreviated by s = singlet, d = doublet, t = triplet, q = quartet, m = multiplet. Combinations of the above are also used, for example dd = doublet-of-a-doublet and td = triplet-of-a-doublet. Liquid-state ^{1}H and ^{13}C NMR spectra are depicted in Fig. S7, ESI.† Solid-state cross-polarisation/magic angle spinning (CP/MAS) experiments were recorded on a Bruker Avance III HD 400 spectrometer. Zirconium oxide rotors were used for sample preparation and spun at MAS rate at 14 kHz. A current pulse program cross-polarisation from ^{1}H to ^{13}C (hC.CP) was conducted using a solid-state PH MAS 400SB BL4-P/H VTN probe tuned and matched at a frequency of 100.6228 MHz. All spectra were recorded at room temperature (298 K) while DQD was used as acquisition mode. Acquisition time was 0.015 s, 2800 scans were used, recycle delay of 5 s, dwell time 5 μs and pre-scan delay DE of 6.505 μs. Pulse parameters were set as P0: 2000 μs, P1: 4.5 μs, P2: 9 μs, P3: 3 μs, P4: 6 μs and P15: 2000 μs.

Elemental microanalysis. Carbon, hydrogen, nitrogen and sulphur (CHNS) analysis (sample was used as is) was performed on an Elementar Analysensysteme varioMICRO V1.6.2 GmbH analysis system.

Mass spectroscopy. High resolution mass spectrometry (see Fig. S8, ESI†) was performed on a Waters Synapt G2 TOF instrument with an ESI source, ESI Pos, Cone Voltage 15 V, Stellenbosch University.

Melting points. Wwere determined on a Reichert Hot-Stage (Protea Holdings Ltd) melting point apparatus and uncorrected.

Electronic spectra. Solution ultraviolet-visible spectra (Fig. S9, ESI†) were recorded on a Varian Cary 500 spectrophotometer. The compounds were dissolved in different solvents which include acetone, DMSO, chloroform and methanol with concentration approximately ≈ 5.0×10^{-4} M. Solid-state

UV-visible absorption spectra (Fig. S10, ESI†) were measured using a PerkinElmer LAMBDA 25 spectrometer.

PXRD measurements. PXRD profiles were recorded on a Bruker D8 Discover X-ray powder diffractometer with a Lynx Eye detector (proportional counter), using Cu Kα radiation (nickel filter, λ = 1.54178 Å). The X-ray or generator tube was operated at 40 kV and a current of 40 mA for 40 minutes. The divergence slit width was 0.5 mm and the primary soller slit 4.0°. The scan rate was 1° min^{-1} and the data was collected for 2θ values of 5 to 50°, except where otherwise indicated.

DSC measurements. Differential Scanning Calorimetry (DSC) profiles, shown in Fig. S11, (ESI†) were collected using a PerkinElmer DSC 6000 differential scanning calorimeter, with Pyris *Version* 4.01 software (instrumental error of ±2%). Samples were weighed between 2–5 mg and a reference was heated from 25 to 445 °C at a rate of 10 °C min^{-1} under a nitrogen atmosphere (flow rate of 19.8 mL min^{-1}). The DSC 2500-TA Instrument was also used (with nitrogen purge at a heating rate of 20 °C min^{-1}) over a wide temperature range of 80–250 °C. The difference in the power supplied to the furnaces of the sample and reference is recorded.

Single-crystal X-ray diffraction. Datasets for **3a_RT** and **3b_LT** were collected at Nelson Mandela University using a Bruker APEX-II CCD diffractometer equipped with graphite monochromated Mo Kα radiation (λ = 0.71073 Å) at **LT** (150 K) and **RT** (298 K). Data reduction was carried out using the Bruker program SAINT.[57] A numerical absorption correction SADABS[58] was applied. The structures of the SA–derivatives were solved using a dual-space algorithm and refined by the full-matrix least-square technique on F^2 with anisotropic thermal parameters to describe the thermal motions of all non-hydrogen atoms using the programs SHELXT–2018/2 (ref. 59) and SHELXL–2018/3 (ref. 60), respectively. The hydrogen atoms of the methyl groups were allowed to rotate with a fixed angle around the C–C bonds to best fit the experimental electron density while all other hydrogen atoms were placed at geometrically idealised positions. The methyl/hydroxyl hydrogen atoms were assigned isotropic temperature factors equal to 1.5 times the equivalent temperature factor of the parent atom whereas the displacement parameters for the other hydrogen atoms were taken as $U_{iso}(H) = 1.2U_{eqv}(C)$.

X-Ray data for **1_RT**, **2_LT**, **2_RT**, **6_LT** and **6_RT** was collected at Rhodes University on a Bruker D8 VENTURE APEX4 AXS area detector diffractometer,[61] equipped with a graphite monochromator and a Mo Kα (λ = 0.71073 Å, at **LT** (150 K) and **RT** (298 K) fine-focus sealed tube operated at 2.0 kW (50 kV, 40 mA). All reflections were emerged and integrated with the Bruker SAINT and XPREP software packages, respectively.[62] Data were collected for absorption effects using the multi-scan techniques SADABS,[63] and the structures were solved by the direct methods package SHELXT and refined using X-Seed software incorporating SHELXL.[64,65] The final anisotropic full-matrix least-squares refinement was done on F^2. The methyl and aromatic protons were placed in geometrically idealised positions (C–H = 0.93–0.98 Å) and constrained to ride on their parent atoms with $U_{iso}(H) = 1.2U_{eqv}(C)$. SHELX constraints and restraints were used to model structures. The non-hydrogen atoms were refined with anisotropic displacement parameters.

Single-crystals of **1_LT**, **4_LT**, **4_RT**, **5_LT**, **5_RT**, **7_LT** and **7_RT** and, variable temperature data sets were collected at University of Pretoria on a Rigaku XtaLAB Synergy R diffractometer equipped with either graphite monochromated Mo Kα radiation (λ = 0.71073 Å) or Cu Kα (λ = 1.54184 Å), with a rotating-anode X-ray source and a HyPix CCD detector. Data reduction and absorption were carried out using the CrysAlisPro (*version* 1.171.40.23a) software package.[66] X-ray diffraction measurements were performed at **LT** (150 K) and **RT** (298 K) using an Oxford Cryogenics Cryostat. All structures were solved by an intrinsic phasing algorithm using SHELXTS[57] and were refined by full-matrix least-squares methods based on F^2 utilizing SHELXL.[58] All non-hydrogen atoms were refined anisotropically while all hydrogen atoms were placed in idealised positions and refined using riding models.

Programs. WINGX,[67] PLATON[68] (for structure validation and geometrical calculation), Mercury,[69] X-Seed,[70] Olex2 (version 1.5)[71] and DIAMOND[72] were used for molecular graphics and refinements while enCIFer[73] was utilised for CIF editing. *PASCal*,[55] a web-based tool, was employed to demonstrate thermomechanical behaviour of the compounds.

CCDC No. 1899401, 1902658, 1966932, 1989369, 1989398, 1989403, 2014911, 2014914, 2019418, 2049690, 2049691, 2062423, 2157376, 2156456–2156467 and 2191107–2191119.[74]

Author contributions

Siya T. Hulushe: conceptualization, data curation, formal analysis, experimental investigation, methodology, validation, visualization, writing – manuscript; Frederick P. Malan: data curation, formal analysis, validation, review, editing manuscript; Eric C. Hosten: data curation, formal analysis, validation; Kevin A. Lobb: data curation, formal analysis, validation; Setshaba D. Khanye: resources, funding acquisition; Gareth M. Watkins: project administration, supervision, funding acquisition.

Conflicts of interest

The authors declare no conflict of interest.

Acknowledgements

The authors thank Distinguished Professor Tebello Nyokong (DST Institute for Nanotechnology Innovation or DST-INI, Rhodes University – South Africa) for allowing us time to use solid-state ultraviolet-visible absorption spectrometer. We are grateful to Dr Xavier Siwe Noundou (Rhodes University, South Africa) for assisting us with solid-state ^{13}C NMR experiments. The authors thank the anonymous reviewers of the New Journal of Chemistry (NJC), whose insightful comments aided us to improve the paper. This work was supported by the National

Research Foundation (NRF), South Africa and Rhodes University Research Council.

References

1 E. Hadjoudis and I. M. Mavridis, *Chem. Soc. Rev.*, 2004, **33**, 579–588.
2 (*a*) E. Hadjoudis, S. D. Chatziefthimiou and I. M. Mavridis, *Curr. Org. Chem.*, 2009, **13**, 269–286; (*b*) A. Carletta, F. Spinelli, S. d'Agostino, B. Ventura, M. R. Chierotti, R. Gobetto, J. Wouters and F. Grepioni, *Chem. – Eur. J.*, 2017, **23**, 5317–5329.
3 B. Rösner, M. Milek, A. Witt, B. Gobaut, P. Torelli, R. H. Fink and M. M. Khusniyarov, *Angew. Chem., Int. Ed.*, 2015, **54**, 12976–12980.
4 T. Mutai, H. Satou and K. Araki, *Nat. Mater.*, 2005, **4**, 685–687.
5 H. Akiyama, A. Sako, N. Tajima, M. Shizuma, R. Kuroda and Y. Imai, *Tetrahedron*, 2016, **72**, 2109–2115.
6 P. T. Todorov, P. N. Peneva, S. I. Georgieva, R. I. Rusew, B. L. Shivachev and A. H. Georgie, *New J. Chem.*, 2019, **43**, 2740–2751.
7 D. R. Kanis, M. A. Ratner and T. J. Marks, *Chem. Rev.*, 1994, **94**, 195–242.
8 N. Prasad and D. J. Williams, *Introduction to Non-linear Optical Effects in Molecules and Polymers*, Wiley, New York, 1991.
9 E. V. Shah and D. R. Roy, *Comput. Mater. Sci.*, 2014, **88**, 156–162.
10 H. Sun, J.-Y. Li, F.-F. Han, R. Zhang, B.-X. Miao and Z.-H. Ni, *Dyes Pigm.*, 2019, **167**, 143–150.
11 M. Ziółek, K. Filipczak and A. Maciejewski, *Chem. Phys. Lett.*, 2008, **464**, 181–186.
12 S. D. Chatziefthimiou, Y. G. Lazarou, E. Hadjoudis, T. Dziembowska and I. M. Mavridis, *J. Phys. Chem. B*, 2006, **110**, 23701–23709.
13 Z. Li, C. Zhang, S. Huang, S. Li, J. Yin and S. Hua Liu, *Mol. Cryst. Liq. Cryst.*, 2012, **557**, 84–89.
14 H. Houjou, H. Ikedo and I. Yoshikawa, *Chem. Commun.*, 2017, **53**, 10898–10901.
15 J. Quertinmont, A. Carletta, N. A. Tumanov, T. Leyssens, J. Wouters and B. Champagne, *J. Phys. Chem. C*, 2017, **121**, 6897–6908.
16 K. Ogawa, Y. Kasahara, Y. Ohtani and J. Harada, *J. Am. Chem. Soc.*, 1998, **120**, 7107–7108.
17 K. Johmoto, T. Ishida, A. Sekine, H. Uekusa and Y. Ohashi, *Acta Crystallogr., Sect. B: Struct. Sci.*, 2012, **68**, 297–304.
18 J. Harada, T. Fujiwara and K. Ogawa, *J. Am. Chem. Soc.*, 2007, **129**, 16216–16221.
19 T. Fujiwara, J. Harada and K. Ogawa, *J. Phys. Chem. B*, 2004, **108**, 4035–4038.
20 Y. Shinde, S. Sproules, L. Kathawate, S. Pal, V. B. Konkimalla and S. Salunke-Gawali, *J. Chem. Sci.*, 2014, **126**, 213–225.
21 F. H. Kamounah, L. Antonov, V. Petrov and G. J. van der Zwan, *J. Phys. Org. Chem.*, 2007, **20**, 313–320.
22 D. Nedeltcheva and L. Antonov, *J. Phys. Org. Chem.*, 2009, **22**, 274–281.
23 A. Afkhami, F. Khajavi and H. Khanmohammadi, *Anal. Chim. Acta*, 2009, **634**, 180–185.
24 T. Steiner and G. Koellner, *Chem. Commun.*, 1997, 1207–1208.
25 H. Pizzala, M. Carles, W. E. E. Stone and A. Thevand, *J. Mol. Struct.*, 2000, **526**, 261–268.
26 B. D. Sharma and J. F. McConnell, *Acta Crystallogr.*, 1965, **19**, 797–806.
27 F. Betchel, J. Gaultier and C. Hauw, *Cryst. Struct. Commun.*, 1973, **2**, 469–472.
28 P. M. Bhatt and G. R. Desiraju, *Chem. Commun.*, 2007, 2057–2059.
29 M. Juribašić, N. Bregović, V. Stilinović, V. Tomišić, M. Cindrić, P. Šket, J. Plavec, M. Rubčić and K. Užarevic, *Chem. – Eur. J.*, 2014, **20**, 17333–17345.
30 J. W. Ledbetter, Jr., *J. Phys. Chem.*, 1968, **72**, 4111–4115.
31 T. Dziembowska, *Pol. J. Chem.*, 1998, **72**, 193–209.
32 J. M. Fernandez-G, F. R. Portilla, B. Q. Garcia, R. A. Toscano and R. Salcedo, *J. Mol. Struct.*, 2001, **561**, 197–207.
33 M. D. Cohen and G. M. J. Schmidt, *J. Phys. Chem.*, 1962, **66**, 2442–2446.
34 J. Bergman, L. Leiserowitz and G. M. J. Schmidt, *J. Chem. Soc.*, 1964, 2068–2085.
35 M. D. Cohen, Y. Hirshberg and G. M. J. Schmidt, *J. Chem. Soc.*, 1964, 2051–2059.
36 M. D. Cohen and G. M. J. Schmidt, *J. Chem. Soc.*, 1964, 2041–2051.
37 M. Zbačnik, K. Pičuljan, J. Parlov-Vuković, P. Novak and A. Roodt, *Crystals*, 2017, **7**, 1–22.
38 E. Hadjoudis, M. Vittorakis and I. M. Mavridis, *Tetrahedron*, 1987, **43**, 1345–1360.
39 V. S. Padalkar and S. Seki, *Chem. Soc. Rev.*, 2016, **45**, 169–202.
40 M. D. Cohen, G. M. J. Schmidt and S. Flavian, *J. Chem. Soc.*, 1964, 2041–2051.
41 F. Robert, A. D. Naik, B. Tinant, R. Robiette and Y. Garcia, *Chem. – Eur. J.*, 2009, **15**, 4327–4342.
42 (*a*) D. A. Safin, K. Robeyns and Y. Garcia, *CrystEngComm*, 2012, **14**, 5523–5529; (*b*) F. Robert, P.-L. Jacquemin, B. Tinant and Y. Garcia, *CrystEngComm*, 2012, **14**, 4396–4406.
43 D. A. Safin, M. Bolte and Y. Garcia, *CrystEngComm*, 2014, **16**, 8786–8793.
44 M. Zbačnik, I. Nogalo, D. Cinčić and B. Kaitner, *CrystEngComm*, 2015, **17**, 7870–7877.
45 M. C. Etter, J. C. MacDonald and J. Bernstein, *Acta Crystallogr., Sect. B: Struct. Sci.*, 1990, **46**, 256–262.
46 M. N. Tahir, H. Ahmad Shad and R. H. Tariq, *Acta Crystallogr., Sect. E: Struct. Rep. Online*, 2011, **67**, o2319.
47 (*a*) N. K. Kaynar, H. Tanak, S. Sahin, N. Dege, E. Ağar and M. Yavuz, *Crystallogr. Rep.*, 2016, **61**, 239–242; (*b*) I. Killic, E. Agar, F. Ersahin and S. Isik, *Acta Crystallogr., Sect. E: Struct. Rep. Online*, 2009, **65**, o737.
48 A. Teimouri, A. N. Chermahini, K. Taban and H. A. Dabbagh, *Spectrochim. Acta, Part A*, 2009, **72**, 369–377.

49 H. A. Dabbagh, A. Teimouri, A. N. Chermahini and M. Shahraki, *Spectrochim. Acta, Part A*, 2008, **69**, 449–459.
50 G. Varasanyi, *Assignments for Vibrational Spectra of Seven Hundred Benzene Derivatives*, Adam Hilger, London, 1974.
51 H. Tanak, *J. Phys. Chem. A*, 2011, **115**, 13865–13876.
52 Ç. Albayrak, G. Kaştaş, M. Odabaşoğlu and R. Frank, *Spectrochim. Acta, Part A*, 2011, **81**, 72–78.
53 (*a*) O. Domínguez, B. Rodríguez-Molina, M. Rodríguez, A. Ariza, N. Farfánc and R. Santillan, *New J. Chem.*, 2011, **35**, 156–164; (*b*) M. Jaworska, P. B. Hrynczyszyn, M. Wełniak, A. Wojtczak, K. Nowicka, G. Krasiński, H. Kassassir, W. Ciesielski and M. J. Potrzebowski, *J. Phys. Chem. A*, 2010, **114**, 12522–12530.
54 (*a*) M. Rubčić, K. Uzžrević, I. Halasz, N. Bregović, M. Mališ, I. Đilović, Z. Kokan, R. S. Stein, R. E. Dinnebier and V. Tomišić, *Chem. – Eur. J.*, 2012, **18**, 5620–5631; (*b*) A. Makal, W. Schilf, B. Kamieński, A. Szady-Chelmieniecka, E. Grech and K. Wózniak, *Dalton Trans.*, 2011, **40**, 421–430; (*c*) J. Sitkowski, L. Stefaniak, I. Wawer, L. Kaczmarek and G. A. Webb, *Solid State Nucl. Magn. Reson.*, 1996, **7**, 83–84; (*d*) S. R. Salman, J. C. Lindon, R. D. Farrant and T. A. Carpenter, *Magn. Reson. Chem.*, 1993, **31**, 991–994; (*e*) H. Saitô, I. Ando and A. Ramamoorthy, *Prog. Nucl. Magn. Reson. Spectrosc.*, 2010, **57**, 181–228.
55 M. J. Cliffe and A. L. Goodwin, *PASCal*: A Principal-Axis Strain Calculator for Thermal Expansion and Compressibility Determination., *J. Appl. Crystallogr.*, 2012, **45**, 1321–1329.
56 B. Nicolaï, I. B. Rietveld, M. Barrio, N. Mahé, J.-L. Tamarit, R. Céolin, C. Guéchot and J.-M. Teulon, *Struct. Chem.*, 2013, **24**, 279–283.
57 Bruker, *SAINT (Version 7.68A)*, Bruker AXS Inc., Madison, Wisconsin, USA, 2012.
58 Bruker, *APEX2 (2011.4-1) and SADABS (Version 2008/1)*, Bruker AXS Inc., Madison, Wisconsin, USA, 2012.
59 G. M. Sheldrick, *Acta Crystallogr., Sect. A: Found. Adv.*, 2015, **71**, 3–8.
60 G. M. Sheldrick, *Acta Crystallogr., Sect. C: Struct. Chem.*, 2015, **71**, 3–8.
61 Bruker, *APEX4, SAINT and SADABS*, Bruker AXS Inc., Madison, Wisconsin, USA, 2021.
62 Bruker, *SAINT-Plus, Version 7.12 (Including XPREP)*, Bruker AXS Inc., Wisconsin, USA, 2004.
63 Bruker, *SADABS, Version 2004/1*, Bruker AXS Inc., Madison, Wisconsin, USA, 1998.
64 O. V. Dolomanov, L. J. Bourhis, R. J. Gildea, J. A. K. Howard and H. Puschmann, *J. Appl. Crystallogr.*, 2009, **42**, 339–341.
65 G. M. Sheldrick, *SHELXL-97, Program for the refinement of crystal structures*, University of Göttingen, Germany, 1997.
66 Rigaku Oxford Diffraction, Rigaku Corporation, Oxford, UK, 2018.
67 L. J. Farrugia, *J. Appl. Crystallogr.*, 2012, **45**, 849–854.
68 A. L. Spek, *PLATON*, molecular geometry program, *J. Appl. Crystallogr.*, 2003, **36**, 7–13.
69 C. F. Macrae, I. J. Bruno, J. A. Chisholm, P. R. Edgington, P. McCabe, E. Pidcock, L. Rodriguez-Monge, R. Taylor, J. van de Streek and P. A. Wood, *J. Appl. Crystallogr.*, 2008, **41**, 466–470.
70 L. J. Barbour, X-Seed, *J. Supramol. Chem.*, 2001, **1**, 189–191.
71 L. J. Bourhis, O. V. Dolomanov, R. J. Gildea, J. A. K. Howard and H. Puschmann, *Acta Crystallogr., Sect. A: Found. Adv.*, 2015, **A71**, 59–75.
72 K. Brandenburg, *DIAMOND*, Crystal Impact, Bonn, Germany, 2005.
73 F. H. Allen, O. Johnson, G. P. Shields, B. R. Smith and M. Towler, *J. Appl. Crystallogr.*, 2004, **37**, 335–338.
74 F. H. Allen, *Acta Crystallogr., Sect. B: Struct. Sci.*, 2002, **58**, 380–388.